Environmental Science
Water Research & Technology

ROYAL SOCIETY OF CHEMISTRY

CRITICAL REVIEW

View Article Online
View Journal | View Issue

Check for updates

Cite this: *Environ. Sci.: Water Res. Technol.*, 2026, **12**, 1048

# Upgrading the two-stage partial nitritation/anammox process: high-rate partial nitritation with hydroxyapatite-enhanced anammox granular sludge

Ying Song,†[a] Lan Lin,†[b] Chao Rong[c] and Yu-You Li *[de]

Two-stage partial nitritation/anammox (PN/A) provides a low-energy, low-carbon pathway for nitrogen removal. In recent years, high-rate partial nitritation coupled with hydroxyapatite (HAP)-enhanced anammox granules has attracted growing attention. This review summarizes current progress and outlines future directions for this process. We first examine the fundamentals of PN and anammox separately, covering reaction stoichiometry and kinetics alongside microbial ecology and practical operating windows. We then discuss the role of HAP in granulation and biomass stabilization, clarifying the proposed mechanisms (*e.g.*, nucleation/templating, Ca–P surface chemistry, and EPS interactions) and the rationale for selecting the HAP-enhanced granules. Next, we compile laboratory and pilot evidence under low-temperature and real-wastewater matrices and assess two-stage coupling, with emphasis on inter-stage load balance and control strategies that deliver the desired $NO_2^-$-N : $NH_4^+$-N ratio to the anammox stage. Finally, we identify key limitations and future needs, which center on the PN step and end-to-end process engineering: robust NOB control with sustained AOB activity at low temperature; predictive, site-transferable approaches for community composition design and process control; and full-chain integration, including pretreatment for complex industrial wastewaters and adaptive cascade control. Overall, this review provides a comprehensive, systematic summary of advantages and research gaps to guide future study and implementation of high-rate PN with HAP-enhanced anammox.

Received 31st August 2025,
Accepted 9th January 2026

DOI: 10.1039/d5ew00850f

rsc.li/es-water

Open Access Article. Published on 05 ubat 2026. Downloaded on 12.05.2026 23:52:08.
This article is licensed under a Creative Commons Attribution-NonCommercial 3.0 Unported Licence.

### Water impact

Utilities and industrial facilities need low-carbon, resilient nitrogen removal systems to directly protect receiving waters and enable water reuse. This review examines a high-rate two-stage partial nitritation process that is coupled with hydroxyapatite-enhanced anammox granules (PN/A). Benefits include reduced aeration and chemicals, a compact footprint, and stable compliance under cold and variable loads. This process could also be used for phosphorus recovery.

## 1 Introduction

The transition to nitrogen removal processes has become a critical focus in wastewater treatment, driven by increasingly stringent discharge standards and sustainability demands.[1,2] Over the past two decades, the PN/A process has emerged as an energy- and resource-efficient alternative to conventional nitrification–denitrification.[3,4] PN/A involves two sequential reactions: the partial oxidation of ammonium to nitrite,[5] followed by the anaerobic conversion of the remaining ammonium and nitrite to dinitrogen gas.[6] This pathway can reduce aeration requirements by approximately 60% and eliminate the need for external organic carbon, making it especially appealing for municipal and industrial wastewater treatment.[7,8] In particular, this review focuses on the context of industrial wastewater, where high-strength nitrogen loads and variable inorganic compositions present unique challenges and create strong incentives for adopting energy-efficient nitrogen removal technologies.

[a] *Zhejiang Key Laboratory of Solid Waste Pollution Control and Resource Utilization, School of Environmental Science and Engineering, Zhejiang Gongshang University, Hangzhou 310012, China*
[b] *Fujian Key Laboratory of Coastal Pollution Prevention and Control, College of the Environment & Ecology, Xiamen University, Xiamen 361102, China*
[c] *School of Energy and Environment, City University of Hong Kong, Hong Kong Special Administrative Region, China*
[d] *Department of Civil and Environmental Engineering, Graduate School of Engineering, Tohoku University, 6-6-06, Aramaki Aza Aoba, Aoba-ku, Sendai, Miyagi 980-8579, Japan. E-mail: gyokuyu.ri.a5@tohoku.ac.jp*
[e] *Graduate School of Environmental Studies, Tohoku University, 6-6-06 Aramaki Aza Aoba, Aoba-ku, Sendai, Miyagi, 980-8579, Japan*
† These authors share first authorship.



This journal is © The Royal Society of Chemistry 2026

Open Access Article. Published on 05 ubat 2026. Downloaded on 12.05.2026 23:52:08.
This article is licensed under a Creative Commons Attribution-NonCommercial 3.0 Unported Licence.

Nevertheless, achieving stable long-term operation of PN/A remains challenging.[9,10] The principal barriers span multiple layers: (i) biochemical constraints: PN/A requires a tight nitrite-to-ammonium supply ratio (~1.32 : 1, mol $mol^{-1}$) to satisfy anammox stoichiometry, while excess nitrite and the free species (FA and FNA) can inhibit either step;[11] (ii) microbial ecological competition: NOB can divert nitrite to nitrate under suboptimal DO, temperature, or FA/FNA windows, undermining partial nitritation;[12,13] (iii) operational strategy: narrow DO–pH–temperature ranges, alkalinity deficits, and influent variability cause oscillations in nitrite production/consumption;[14] (iv) matrix effects: residual organics and competing electron acceptors perturb nitrite availability and anammox performance;[15–17] (v) environmental stressors: low temperatures depress PN and anammox kinetics and slow start-up;[18,19] (vi) inhibitory contaminants: heavy metals, antibiotics, sulfide, and oxidants impair activity;[20–24] (vii) reactor-scale limitations: slow anammox growth, biomass washout risk, granule disintegration, and mass-transfer limitations in dense biofilms;[25] and (viii) interstage load imbalance in two-stage configurations: a commonly observed case is insufficient PN capacity relative to anammox demand, leading to $NO_2^-$ limitation, $NH_4^+$ breakthrough, and underloaded anammox despite available reactor capacity.[26]

Beyond process configuration, the application of MIM has emerged as an effective strategy to reinforce sludge structure and enhance process resilience.[27,28] Different types of minerals, such as calcium carbonate and iron-based compounds, have been shown to provide nucleation sites, strengthen EPS networks, and improve sludge granulation and settleability.[29,30] Comparative studies highlight that these biomineralization pathways can increase biomass retention and tolerance to stress conditions.[31,32] Within this broader context, HAP, a calcium phosphate mineral, has received particular attention.[33–35] In addition to its favorable physicochemical properties that promote granulation and biomass stabilization, the interest in HAP also stems from its economic feasibility in calcium addition and its compatibility with typical wastewater matrices, where $Ca^{2+}$ and $PO_4^{3-}$ are common inorganic constituents.[36,37] Notably, many industrial wastewaters, such as those from food processing and fermentation, contain relatively high levels of Ca and P, providing a naturally favorable environment for *in situ* HAP formation and thus further facilitating mineral-induced granulation.[38] Evidence further indicates that HAP supplementation not only accelerates anammox granule development but also enhances system performance under challenging conditions, such as low temperature and real wastewater treatment.[39–41]

In this review, we first examine the fundamentals of PN and anammox separately, including reaction stoichiometry/kinetics *vs.* microbial ecology and operating windows. We then discuss the role of HAP in granulation and biomass stabilization, clarifying mechanisms and selection rationale. Next, we compile laboratory and pilot evidence under low-temperature and real wastewater matrices and assess two-stage coupling with an emphasis on inter-stage load balance. Overall, this work provides a comprehensive, systematic summary of the process's advantages and the key research needs, with the aim of guiding future studies and implementation.

## 2 Methodology

This review was carefully structured to provide a critical synopsis of recent advances in two-stage partial nitritation–anammox processes, with a particular emphasis on HAP-enhanced anammox granular sludge. The organization of the review is as follows: (1) introduce the fundamentals of partial nitritation and anammox processes, and highlight the potential roles of HAP in facilitating granular sludge development; (2) examine laboratory-scale investigations and pilot-scale applications of high-rate PN and HAP-assisted anammox processes, and summarize the operational strategies, benefits, challenges, and potential solutions; (3) evaluate the overall performance and integration of two-stage PN/HAP–anammox systems; and (4) provide insights into limitations and future perspectives for upgrading this approach.

A systematic literature search was carried out using major scientific databases, including Web of Science, Scopus, ScienceDirect, and Google Scholar. The primary keywords included combinations such as "partial nitritation", "nitritation", and "hydroxyapatite + anammox". In a second step, the search was refined to focus on more specific aspects relevant to this review, such as "low-temperature anammox", "granule formation and stability", "mineral-assisted anammox", "microbial community structure", "real wastewater performance", and "process integration", Search strings were adjusted according to the syntax of each database to ensure comprehensive coverage. For PN, this review primarily focuses on studies published within the past five years (2021–2025), which best reflect recent technological advancements and operational strategies. In contrast, research specifically addressing HAP-enhanced anammox processes remains relatively limited. Therefore, while this review also emphasizes studies from the past five years, several influential earlier publications from 2018–2019 are included due to their foundational contributions to understanding HAP–microbial interactions and anammox granule stability. All collected references were imported into Mendeley for further screening and classification. The filtering was conducted in three stages: (1) removal of duplicates and non-peer-reviewed documents, with only English-language publications retained; (2) preliminary screening by title and abstract to exclude irrelevant works; (3) detailed reading and classification of the remaining articles according to research focus (fundamentals, laboratory studies, pilot/full-scale applications, and process evaluations).

Open Access Article. Published on 05 ubat 2026. Downloaded on 12.05.2026 23:52:08.
This article is licensed under a Creative Commons Attribution-NonCommercial 3.0 Unported Licence.

It should be noted that some relevant studies may not have been included, particularly those published in non-English journals or that are not publicly accessible. Moreover, this review focuses on process fundamentals, laboratory investigations, and engineering applications of two-stage PN/HAP–anammox systems. Broader aspects, such as life cycle assessment, economic analysis, and full-scale techno-economic feasibility studies, are beyond the scope of this work.

# 3 Fundamentals of two-stage PN/HAP–anammox

## 3.1 Partial nitritation

**3.1.1 Reaction pathways and microbial ecology.** Ammonia-oxidation in engineered N-cycling systems proceeds *via* four canonical routes: nitritation, nitratation, two-step nitrification, and comammox. Their net reactions, mediating enzymes, and representative taxa are summarized in Table 1. These pathways differ not only in thermodynamics and electron-transfer biochemistry but also in ecophysiology—substrate and $O_2$ affinities, growth yields, and habitat preferences in flocs, biofilms, and granular sludge, which in turn define distinct operational levers in reactors.[42–44] This review centers on nitritation because it is intentionally coupled with anammox in two-stage trains to minimize aeration and alkalinity demands while avoiding excess $NO_3^-$ formation. The core objective of nitritation is to successfully suppress NOB while maintaining the activity of AOB.

**3.1.2 Kinetic fundamentals.** Suppressing NOB relies on two complementary principles: exploiting kinetic differentials (growth-rate contrasts) and reshaping the resource landscape (substrate and oxygen affinities and availabilities). Growth-rate advantages are context-dependent, being jointly governed by temperature, pH, substrate levels, and inhibitory factors, so practice has moved beyond single-parameter tuning to integrated, multi-parameter control designed to sustain NOB suppression over long operation.

*3.1.2.1 Temperature and yields.* Temperature governs intrinsic kinetics of AOB, NOB, comammox, and AOA through enzyme rates, maintenance, diffusion, and acid–base speciation. It is reported that $\mu_{AOB}$ was in the range of 1.07–1.12 $d^{-1}$ and $\mu_{NOB}$ was in the range of 1.05–1.09 $d^{-1}$. Thus, a 10 °C warming from 15 to 25 °C can increase AOB rates by 1.9–3.1 times and NOB by 1.6–2.4 times, and the AOB : NOB rate ratio increases by roughly 20% if $\mu_{AOB}$ is 1.09 $d^{-1}$ and $\mu_{AOB}$ is 1.07 $d^{-1}$.[45,46] With a median $\mu_{max}$ of 0.67 $d^{-1}$ for NOB and 1.0 $d^{-1}$ for AOB at temperatures above 30 °C, NOB can be effectively washed out by SRT control. With a median $\mu_{max}$ of ~1.0 $d^{-1}$ for AOB and ~0.67 $d^{-1}$ for NOB at >30 °C, an SRT window typically exists in which AOB are retained while NOB are lost, making washout feasible at solid ages on the order of 1–2 days when decay is modest.[47] This strategy, however, is temperature-limited: as temperature drops into the low-to-mid 20 °C range, the gap narrows, decay and maintenance terms shift, and the SRT window can shrink or vanish.

Beyond the effects on $\mu_{max}$, temperature also modifies the apparent affinities through changes in diffusivity and oxygen solubility, and it shifts substrate speciation ($NH_3/NH_4^+$ and $HNO_2/NO_2^-$), thereby altering the effective saturation and inhibition terms in dual-substrate kinetics.

*3.1.2.2 Substrate affinity.* Substrate affinity describes how effectively a microorganism can capture and utilize its food source, especially when it is scarce. In microbial kinetics, affinity is quantified by the $K_s$. This concept is crucial for understanding microbial competition. In a low-substrate environment, the organism with the highest affinity (lowest $K_s$) will have a significant competitive advantage and will likely become the dominant species. Comammox bacteria, such as *Nitrospira inopinata*, are high-affinity specialists. With an exceptionally low $K_s$ of 0.015 mg N per L,[48] they are adapted to thrive in environments where ammonia is extremely limited, such as in drinking water systems or the final polishing stages of wastewater treatment. AOB such as *Nitrosomonas europaea* have a moderate $K_s$ of 1.62 mg N per L. This makes them well-suited for typical municipal wastewater treatment plants, where ammonia concentrations are higher and more consistent.[49] Moreover, *Nitrosomonas* lineages exhibit disparate apparent affinities: reported $K_s$ values are 0.5–1.6 mg N per L for *N. europaea*,[50] 0.48 mg N per L for *N. oligotropha*,[51] and up to 29.65 mg N per L for other *Nitrosomonas* lineages.[52] It also should be noted that affinity is not a fixed property of "AOB" but an emergent outcome of lineage, environment, and microstructure of the sludge. Accordingly, reported $K_s$ can vary by orders of magnitude across systems, so it should be treated as a system-level property rather than a species constant.

*3.1.2.3 $O_2$ affinity.* Reported $K_o$ values for AOB span over an order of magnitude. *Nitrosospira* spp. show very low $K_o$ (0.10 mg $L^{-1}$),[53] indicating high $O_2$ affinity. *N. europaea* exhibits moderate $K_o$ (0.24–0.41 mg $L^{-1}$),[54,55] while *N. oligotropha* is

**Table 1** Ammonia-oxidation pathways, net reactions, key enzymes and representative microbes

| Pathway | Net reaction | Key enzymes | Representative microbes |
|---|---|---|---|
| Nitritation (ammonia → nitrite) | $NH_4^+ + 1.5O_2 \rightarrow NO_2^- + 2H^+ + H_2O$ | AMO/HAO | AOB: *Nitrosomonas*, *Nitrosospira* AOA: *Nitrosopumilus*, *Nitrososphaera* |
| Nitratation (nitrite → nitrate) | $NO_2^- + 0.5O_2 \rightarrow NO_3^-$ | NXR | NOB: *Nitrospira*, *Nitrobacter*, *Nitrotoga*, *Nitrococcus* |
| Nitrification (nitritation + nitratation) | $NH_4^+ + 2O_2 \rightarrow NO_3^- + 2H^+ + H_2O$ | AMO/HAO (AOB) + NXR (NOB) | *Nitrosomonas*, *Nitrosospira*, *Nitrospira*, *Nitrobacter*, *Nitrotoga*, *Nitrococcus* |
| Comammox (complete ammonia oxidation) | $NH_4^+ + 2O_2 \rightarrow NO_3^- + 2H^+ + H_2O$ | AMO/HAO + NXR (in one genome) | Comammox *Nitrospira* |

 This journal is © The Royal Society of Chemistry 2026

Open Access Article. Published on 05 ubat 2026. Downloaded on 12.05.2026 23:52:08.
This article is licensed under a Creative Commons Attribution-NonCommercial 3.0 Unported Licence.

higher at 1.22 mg $L^{-1}$,[56] consistent with lower $O_2$ affinity. Among non-bacterial ammonia oxidizers, AOA (*Nitrososphaera gargensis*) fall in the low range (0.13–0.21 mg $L^{-1}$).[57] Like $K_s$, the apparent $K_o$ is not purely intrinsic: it increases in thick biofilms or large granules where diffusion limits $O_2$ delivery to inner cells, and it decreases in thin flocs/films where external mass-transfer resistance is small.[34]

### 3.2 Hydroxyapatite (HAP)-enhanced anammox process

#### 3.2.1 Structure and formation mechanism of HAP-enhanced anammox granular sludge

*3.2.1.1 Physicochemical properties of HAP.* Hydroxyapatite (HAP, $Ca_{10}(PO_4)_6(OH)_2$) represents the most thermodynamically stable phase of calcium phosphates, and it is generally formed through the transformation of amorphous or metastable precursors such as ACP, DCPD, OCP, and TCP.[58] Its crystalline structure provides a stable and insoluble framework under neutral to slightly alkaline conditions. Across the neutral pH typical of anammox operation (7.5–8.5), HAP particles generally exhibit a net negative zeta potential, which has been measured to be around mildly negative values in electrolytes and becomes more negative with increasing pH; similar behavior is seen for Ca–phosphate precipitates formed for P recovery from aqueous media. Such surface charge characteristics influence the ability to interact with surrounding dissolved ions or organic macromolecules.[59] In wastewater environments, the effective surface charge of HAP is further modulated by competitive ion adsorption (*e.g.*, $Ca^{2+}$/$Mg^{2+}$ and $PO_4^{3-}$/$CO_3^{2-}$), which also influences nucleation and crystal growth.[34]

HAP precipitates usually present as intergrown microcrystals or loosely aggregated pellets, with a specific surface area that typically ranges from a few to several tens of $m^2$ $g^{-1}$, depending on crystallite size and aggregation state.[60,61] The rough, irregular carrier surface at the microscale favors microbial adhesion and serves as nucleation sites for the aggregation of anammox bacteria and their supporting microorganisms.[62] In addition, HAP contributes phosphate-based buffering capacity to the microenvironment, and quantitative titration on HAP–anammox granules reveals a measurable acid neutralization capacity that helps maintain pH within the anammox-favorable range.[34]

*3.2.1.2 Mechanisms of HAP–microbe interactions.* In anammox reactors treating wastewaters that are rich in Ca–P–N, HAP and biofilms co-assemble through coupled biomineralization and chemical precipitation. The anammox pathway (eqn (1)) tends to slightly elevate local pH near cell surfaces, creating micro-alkaline niches.[63] Under such conditions, supersaturated $Ca^{2+}$ and phosphate ions initially precipitate as amorphous Ca–P (ACP), a poorly ordered and non-stoichiometric precursor. ACP commonly appears in several compositional forms, which can be generically represented by eqn (2). These amorphous phases subsequently transform into crystalline HAP under sustained alkaline microenvironments and in the presence of microbial activity.[58] The net crystallization reaction is given in eqn (3). The ACP → HAP conversion typically proceeds through dissolution-reprecipitation or by solid-state structural rearrangement on existing nuclei, as widely observed in Ca–P mineralization systems.[64,65] This conversion is promoted by sustained alkaline microenvironments, carbonate-equilibrium shifts, and organic matrices (*e.g.*, EPS and cell surfaces) that provide nucleation sites and kinetic facilitation; similar roles of organic scaffolds and microenvironmental regulation in guiding ACP crystallization have been demonstrated in biomineralization studies.[66]

The newly formed HAP then provides nuclei and rigid scaffolds that further stabilize the bioaggregate,[25] creating a positive feedback between mineral precipitation and biofilm growth (Fig. 1). Microscale imaging consistently shows a core-shell architecture in which a porous HAP-rich core is interwoven with biomass, overlain by an active anammox biofilm of regulated thickness (≈0.1–0.6 mm),[31] a structure associated with improved settleability and mass-transfer control. Notably, bulk pH, carbonate equilibrium, and supersaturation are critical factors for the formation and stability of Ca–P phases in reactors.[67,68]

$$1.0NH_4^+ + 1.32NO_2^- + 0.066HCO_3^- + 0.13H^+ \rightarrow 1.02N_2 + 0.26NO_3^- + 0.066CH_2O_{0.5}N_{0.15} + 2.03H_2O \quad (1)$$

$$3Ca^{2+} + 2PO_4^{3-} + nH_2O \rightarrow Ca_3(PO_4)_2{\cdot}nH_2O \quad (2)$$

$$10Ca^{2+} + 6PO_4^{3-} + 2OH^- \rightarrow Ca_{10}(PO_4)_6(OH)_2 \quad (3)$$

EPS play a central role in mineral encapsulation and cohesion within HAP–anammox granules. Divalent cations, particularly $Ca^{2+}$, released and redistributed during Ca–P cycling, can bridge negatively charged functional groups on EPS macromolecules (*e.g.*, carboxyl and phosphorylated groups), thereby neutralizing surface charges, promoting microbial adhesion, and strengthening aggregate cohesion and shock resistance.[69,70] Beyond such direct binding effects, $Ca^{2+}$ also regulates the composition and structure of EPS. Its supplementation has been shown to shift the balance between tightly bound and loosely bound fractions and to alter the PN/PS ratio, thereby modifying the hydrophobicity and flocculation potential of anammox granules.[71,72] In HAP–anammox systems, these EPS–cation interactions further facilitate the encapsulation of mineral phases and drive size-dependent stratification, yielding a core–shell structure with a mineral-rich inner core and an active anammox biofilm on the outer layer.[34,73] Collectively, these findings support the view that EPS–mineral–cation interactions act cooperatively to shape the structural integrity and resilience of HAP–anammox granules.

In addition to providing a stable core–shell architecture, evidence suggests that mature Ca–P-based anammox granules may also serve as a source of renewal for the microbial population. Microscale observations have reported

Open Access Article. Published on 05 ubat 2026. Downloaded on 12.05.2026 23:52:08.
This article is licensed under a Creative Commons Attribution-NonCommercial 3.0 Unported Licence.

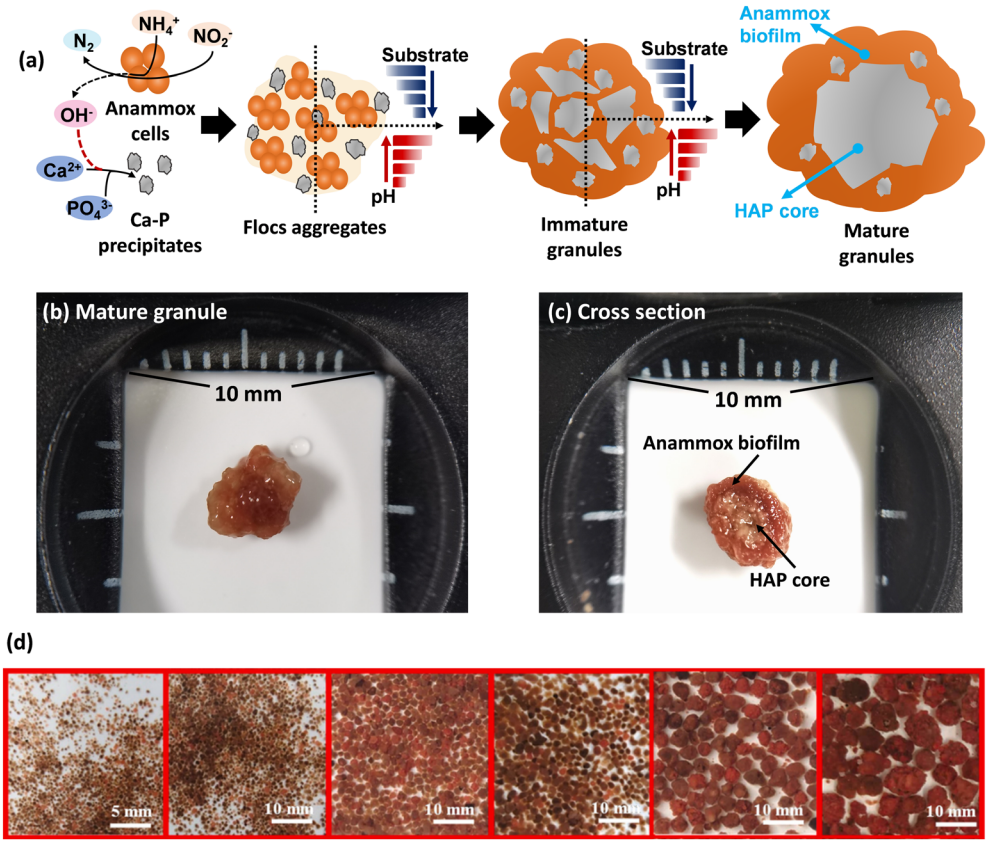


Fig. 1 Schematic of the formation of the HAP–anammox granules (a), photograph of a mature granule (b), and cross-sectional view of a granule (c), photographs of the HAP–anammox granules with different sizes (d).

the detachment of small mineral–biofilm fragments from the surface of larger granules, often comprising hydroxyapatite, EPS, and active bacterial cells.[25,74] These fragments can act as secondary nuclei for the initiation of new granules,[75,76] thereby contributing to population-level stability and resilience under fluctuating operational conditions. This phenomenon underscores the ecological significance of mineral-biofilm interactions, whereby HAP not only contributes to structural stability but also enables continuous renewal of the anammox population.

*3.2.1.3 Functional roles of HAP in anammox granular sludge.* *In situ* precipitation of HAP contributes to the initiation of anammox granulation. Early-formed Ca–P nuclei (as ACP or poorly crystalline Ca–P) can serve as heterogeneous nucleation sites that reduce the energy barrier for microbial aggregation and favor attachment of flocs and micro-colonies, effectively converting flocculent biomass into compact aggregates.[25,77] Moreover, *in situ* HAP formation creates a self-reinforcing loop: mineral nuclei accelerate biomass aggregation, which in turn modifies the local microchemistry (*e.g.* by elevating the pH), thereby favoring further Ca–P precipitation and granule maturation.[78]

In addition to *in situ* precipitation, pre-existing HAP particles can also function as mineral nuclei and rigid scaffolds that accelerate granulation.[79] Their addition has been shown to shorten the granulation period and promote a rapid increase in nitrogen removal rates, while microscopic analyses have revealed HAP–microbe co-aggregation during granule evolution.[80] Nevertheless, in practice, *in situ* HAP formation is typically driven by the need for phosphorus removal and recovery, and the decision between stimulating *in situ* HAP precipitation and dosing pre-existing HAP can be strategically adjusted to balance granulation efficiency with overall process performance.

The formed HAP–anammox granules exhibit clear advantages in settleability, mechanical strength, and biomass retention, compared with conventional anammox granules.[58] Quantitative measurements have shown that mature HAP–anammox granules can reach settling velocities as high as ~360 m $h^{-1}$,[39] with average values consistently exceeding 300 m $h^{-1}$ under optimal calcium/phosphate conditions,[81] far greater than the ~50–100 m $h^{-1}$ typical of non-mineralized anammox granules.[82,83] Mechanically, apatite accumulation within granules provides structural reinforcement, and compression tests and crystallographic evidence have confirmed that apatite-rich anammox granules possess significantly enhanced rigidity and shear resistance.[29] In the anammox granulation process enhanced by externally added HAP particles, the mechanical strength of the sludge increased by 29.6–59.7% by day 180 compared to the early stage.[80] These effects are further amplified by EPS–HAP interactions, where $Ca^{2+}$ bridging and mineral encapsulation


This journal is © The Royal Society of Chemistry 2026

Open Access Article. Published on 05 ubat 2026. Downloaded on 12.05.2026 23:52:08.
This article is licensed under a Creative Commons Attribution-NonCommercial 3.0 Unported Licence.

strengthen the aggregate framework and mitigate disintegration under hydraulic stress.[34]

Importantly, HAP also contributes to biomass retention and long-term stability by shaping a dense mineral core overlain with active biofilm, which helps minimize biomass washout while maintaining high anammox activity.[31,84] The biomass concentration in the reactor increased from 28.3 to 39.4 g $L^{-1}$ with the pre-added HAPs, demonstrating effective microbial retention and enrichment facilitated by HAPs serving as a skeletal structure and cross-linker.[80]

However, although the beneficial role of HAP in strengthening the anammox process is evident, its uncontrolled accumulation may introduce operational drawbacks. Evidence from single-stage anammox–HAP systems shows that prolonged mineral deposition, although favorable for HAP mineral recovery, can shift sludge composition toward highly mineralized aggregates, triggering excessive biomass purge and suppressing microbial activity.[77] Similar patterns have been observed in which increasing inorganic precipitation, reflected in declining VSS/TSS ratios, corresponds to reduced biomass-specific activity in anammox granules, likely as a result of impaired mass transfer and constrained metabolic functioning.[85] These findings suggest that excessive HAP input can drive the system toward a condition where mineral accumulation surpasses microbial growth. As this imbalance develops, the fraction of active biomass declines, diffusion pathways become increasingly restricted, and changes in granule density and settling behavior may ultimately perturb reactor hydraulics.[86] Therefore, while HAP addition facilitates P retention and granulation, sustained benefits require maintaining controlled mineralization through monitoring inorganic content, optimizing $Ca^{2+}$/P dosing, and implementing timely biomass withdrawal to prevent progressive deterioration of sludge activity and stability.[87]

### 3.2.2 Microbial ecology and functional interactions in HAP–anammox granules

*3.2.2.1 Dominant anammox bacteria.* Two-stage HAP–anammox processes have typically identified *Candidatus Kuenenia* as the dominant anammox lineage, both in enrichment systems using synthetic wastewater and during the treatment of real wastewater.[40,88] This contrasts with many conventional anammox enrichments and reactors, which tend to display higher proportions of *Candidatus Brocadia* or mixed anammox populations.[89–91] Moreover, HAP–anammox granules characteristically host highly enriched anammox populations. Within synthetic wastewater cultivation, the bacterial abundance within HAP–anammox granules can reach as high as 47.0%.[92] Even under extremely low-temperature conditions, HAP–anammox granules maintain a high dominance of *Candidatus Kuenenia*, with abundances ranging from 35.3% to 39.1%,[39,87] highlighting the selective advantage provided by HAP-mediated niches. Notably, in real wastewater treatment scenarios, HAP–anammox granular systems typically support *Kuenenia* abundances above 35%, with maxima reaching 57.1%,[11,93] indicating a robust capacity for biomass enrichment and adaptation to complex environmental conditions.

*3.2.2.2 Interactions of anammox bacteria with other microorganisms.* In HAP–anammox granules, anammox bacteria form tightly organized consortia with specific heterotrophic taxa, a pattern driven by the mineral–biofilm architecture created during HAP-mediated granulation.[11,94] The porous HAP core and surrounding biofilm establish a core–shell microscale structure that concentrates anammox cells while creating adjacent niches for heterotrophs involved in EPS turnover and organic scavenging.[95] Filamentous and fermentative members of *Chloroflexi* are commonly enriched in these granules and act as structural scaffolds and hydrolyzers, degrading cell debris and EPS-derived polymers into low-molecular-weight substrates that support community-level recycling and matrix renewal.[96,97] *Proteobacterial* lineages are repeatedly detected at the granule periphery and appear to consume endogenous organics and anammox-derived oxidized nitrogen species, thereby shaping local nitrite/nitrate availability and indirectly modulating anammox activity.[97,98] Notably, specific taxa such as *Candidatus Desulfobacillus denitrificans* have been reported to co-occur and increase markedly in relative abundance alongside anammox organisms in granular systems under certain acclimation conditions,[80] suggesting close ecological associations that may involve denitrification, metabolite exchange, or niche complementarity.[99] In short, the heterotrophic activities of metabolite degradation, provision of structural support, and nitrate/nitrite consumption are spatially organized within HAP-mediated granules, thereby enhancing biomass retention, cross-feeding, and the resilience of anammox-based nitrogen removal in complex wastewaters.

*3.2.2.3 Granule community stability.* HAP-associated granules concentrate a core set of metabolic capacities, such as anammox catabolism, EPS production/degradation, and heterotrophic organic scavenging, which persist under various operational stresses.[100] Experimental studies show that this functional core, evidenced by the dominance of anammox bacteria and key functional gene signatures, is maintained even during exposure to low temperatures and variable loading conditions.[39,101] This functional stability enables sustained nitrogen-removal rates and confers greater resilience to short-term perturbations, such as substrate shocks and transient pH inhibition.[92,102]

Evidence for this stability comes from a study where rapid acclimation to dewatered fermentation liquid was achieved using cold-stored HAP–anammox granules.[40] Within two months, the reactor achieved an increase in the nitrogen removal rate to 5.5 g N per L $d^{-1}$, alongside the maintenance of *Candidatus Kuenenia* dominance (31.1% relative abundance) and a rise in co-occurring taxa such as *Candidatus Desulfobacillus denitrificans* and *Candidatus Nitrosymbiomonas proteolyticus*, demonstrating both functional recovery and community co-enrichment in HAP granules.

Open Access Article. Published on 05 ubat 2026. Downloaded on 12.05.2026 23:52:08.
This article is licensed under a Creative Commons Attribution-NonCommercial 3.0 Unported Licence.

Long-term preservation tests further support the operability and resilience of HAP–anammox granules. In an investigation of stored HAP granules (storage up to six years), careful preservation (4 °C with 5 mM molybdate) limited blackening and reduced decay of SAA, with SAA retention >50% after 6 months and 10% after 1 year. Although functional gene profiles shifted with storage conditions, a retained functional core and measurable recovery potential were observed upon reactivation. These results indicate that HAP–anammox granules have practical long-term storage potential and can support rapid restart when conditions are controlled.

# 4 Lab performance and applications

## 4.1 Partial nitritation

**4.1.1 Reactor configurations and performance.** From a biomass-growth perspective, two-stage PN/A technologies comprise suspended-growth, biofilm (attached-growth), and hybrid modes. The suspended-growth platforms comprised roughly 65% of installations in 2020, compared with ~29% for biofilm systems.[46] To enable cross-study comparison, we summarize recent PN literature (past 2–5 years) by reactor type, sludge type, operational parameters, and performance (Table 2 and Fig. 2). The results showed the operating windows that are broadly comparable: temperatures mostly 22–30 °C (reported range ≈ 11–36 °C), influent nitrogen from municipal-strength to high-strength leachates and liquors (20–2600 mg N per L), typical NLR of 0.1–1.5 g N per L $d^{-1}$ with outliers up to 4.8–5.6 g N per L $d^{-1}$ on mature leachate/dewatering liquors, and HRTs commonly 5–24 h (extended to ~132 h in conservative continuous-flow designs). Reported nitritation performance is generally robust—nitrite production on the order of 30–70% and low nitrate slip under optimized control. Also, the literature uses 'NAR' inconsistently (ratio *vs.* rate), necessitating an explicit definition to enable valid comparisons.

**4.1.2 Challenges and potential solutions.** Here, we highlight three recurring bottlenecks for the PN step in two-stage PN/A systems. First, insufficient loading: conservative HRTs, limited oxygen transfer, and weak AOB retention constrain the attainable NLR. Second, unreliable NOB suppression: particularly at low temperature or under long SRTs, nitrite accumulation erodes as NOB acclimate even under ostensibly low-DO conditions. Third, imprecise control of the effluent ratio R ($NO_2^-$-N : $NH_4^+$-N): analyzer lag and process dead time (often coupled to FA/FNA–pH dynamics) induce oscillations. These challenges are interdependent because measures that raise the rate can weaken suppression or destabilize R. Therefore, solutions must be co-designed across hydraulics, biomass retention, and control architecture. Below, we summarize recent practical countermeasures for each challenge.

*4.1.2.1 Insufficient loading.* Acidic partial nitritation operated under dynamic pH offers a fast, selective lever for NOB control while expanding the attainable loading envelope. By cycling pH (≈7.0 → 4.5) to generate transient *in situ* FA/FNA windows, recent SBR studies achieved stable $NO_2^-$ accumulation (>80%) even at low $NH_4^+$ (~100 mg N per L), with AOB (*Nitrosospira*/*Nitrosomonas*) maintained and NOB failing to adapt—even under high DO (>4 mg $L^{-1}$).[103] A complementary variant exploits self-acidification by *Nitrosomonas* to create, within one cycle, a weakly acidic high-rate AOB window followed by a strongly acidic high-FNA window, and occasional FA shocks reset emerging NOB.[104]

Controlling effective sludge concentration—with emphasis on the active AOB inventory—addresses loading and provides a structural background for NOB suppression. Air-lift reactors

Table 2 The operational setup and performance of the partial nitritation process

| Reactor type | Sludge type | Target wastewater | Temp. °C | Scale L | Nitrogen conc. mg N per L | NLR g N per L $d^{-1}$ | NAR g N per L $d^{-1}$ | HRT h | Nitrite production % | Ref. |
|---|---|---|---|---|---|---|---|---|---|---|
| SBR | Floc | Municipal wastewater | 23–25 | Reactor: 1.5 | $NH_4^+$: 1911 ± 89 | 0.39–0.43 | 0.13–0.25 | 25–50 | 35–59 | 139 |
| SBR | Floc | Synthetic wastewater | 25 | Reactor: 6 | $NH_4^+$: 71–531 | 0.01–0.33 | 0.01–0.14 | 24–144 | 21–63 | 103 |
| SBR | Floc | Artificial (urea + tap water) | 30 | Reactor: 3 | Urea: 500–1200 | 0.23–0.56 | n.a. | 12 | n.a. | 137 |
| n.a. | Floc | Sanitary landfill leachate | 25 | Reactor: 2 | $NH_4^+$: 500–1000 | 0.02–0.17 | 0.05–0.07 | 24 | 30–50 | 108 |
| CFB | Floc | Landfill leachate | 28 ± 2 | Reactor: 60 | $NH_4^+$: 1463 | 0.27 | 0.11 | 132 | 41 | 113 |
| SBR | Floc | Mature landfill leachate | n.a. | Reactor: 0.3 | $NH_4^+$: 1995 $NO_3^-$: 22 | 2.17–5.58 | 0.86–1.56 | 8–24 | 29–78 | 138 |
| ALR | Floc | Fermentation wastewater | 25–30 | Reactor: 4 | $NH_4^+$: 252–1361 | 0.30–1.50 | 0.10–1.40 | 12–48 | 50 | 26 |
| SBR | Floc | Dewatering liquor | 30 | Reactor: 3 | $NH_4^+$: 1420–2600 | 4.80 | 2.40 | 6–24 | 50 | 24 |
| ALR | Floc | Digestate wastewater | 30–35 | Pilot-scale reactor: 20 000 | $NH_4^+$: 373–1734 | 0.21–0.62 | 0.13–0.37 | 43–70 | 56–60 | 123 |
| cf-SBR | Floc | Pre-treated potato wastewater | 23 | Pilot-scale reactor: 60 | TN: 289 ± 34 | 0.16–0.80 | n.a. | n.a. | n.a. | 8 |
| SBR | Biofilm + floc | WWTP | 34 | Full-scale influent: 5 000 000 | $NH_4^+$: 341 ± 46 | 0.23–0.30 | n.a. | 31 | n.a. | 134 |
| AGR | Floc | WWTP | n.a. | Full-scale reactor: 638 000 | TN: 600–1249 | 0.73–1.52 | 0.32–0.73 | 20 | 45–50 | 23 |
| SBR | n.a. | Reject water | 34–36 | Full-scale influent: 400 000 | $NH_4^+$: 1861 ± 164 | 0.76 | 0.21 | 68 | 32 | 2 |

 This journal is © The Royal Society of Chemistry 2026

Open Access Article. Published on 05 ubat 2026. Downloaded on 12.05.2026 23:52:08.
This article is licensed under a Creative Commons Attribution-NonCommercial 3.0 Unported Licence.

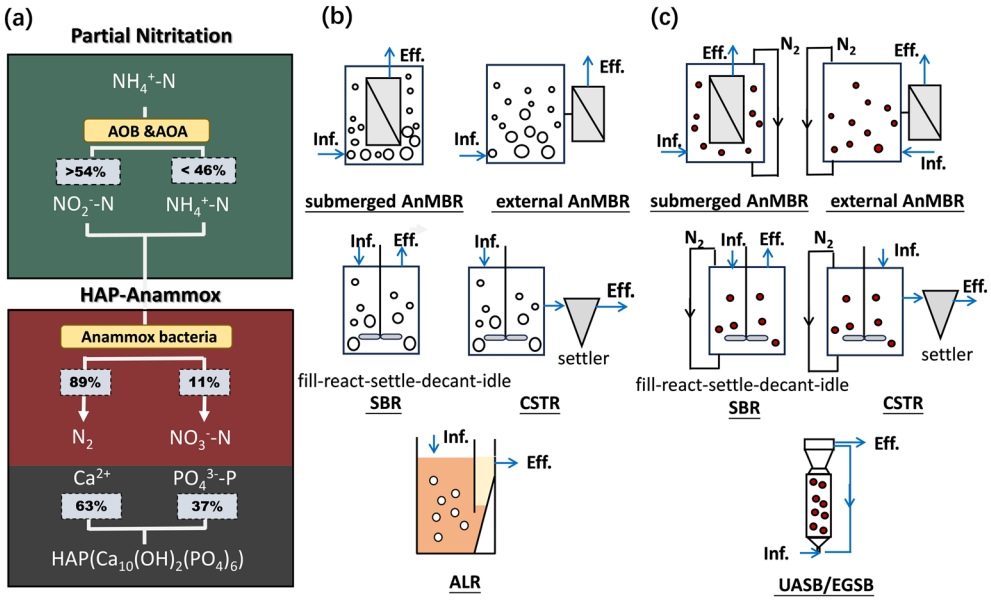


Fig. 2 Schematic of the reaction flow of two-stage PN/HAP–anammox: (a) reactor configurations for PN (b) and reactor configurations for HAP–anammox (c).

are well-suited for this purpose:[11,14] gas-lift hydrodynamics supply high oxygen transfer with uniform, moderate shear, promoting compact aggregates and high biomass retention while allowing bulk SRT to be held just above AOB washout.[11] In prior operations, AOB relative abundance reached ~30%, and NLR approached ~9 g N per L $d^{-1}$ after extended cultivation and operational optimization.

*4.1.2.2 NOB suppression.* At *ca.* 30 °C, SRT-based washout control is generally effective for restraining NOB and sustaining stable nitritation. By contrast, NOB suppression at low temperature is notoriously difficult.[105] Despite $\mu_{NOB} > \mu_{AOB}$ at low temperature, intensive control of DO, FA and FNA can still favor AOB while constraining NOB.[106,107]

FA and FNA are consistently identified as major routes for selective NOB repression.[108] Short-pulse exposures can limit NOB more than AOB—for example, a 6 h FA treatment at ~16.8 mg $NH_3$ per L under anoxic conditions reduced AOB activity by ~16% but NOB by ~29%.[109,110] By contrast, chronic or overly intense FA application can trigger community replacement (*e.g.*, *Nitrospira* → *Nitrotoga*) and loss of suppression[111] consistent with the view that NOB lineages can adapt to distinct FA/FNA stresses.[112] In practice, transient, well-timed FA/FNA windows (*e.g.*, *via* dynamic pH) are preferable to sustained exposure and should be coordinated with DO/SRT control.[113]

Transport constraints strongly condition NOB control. In immobilized-cell matrices, steep $O_2$ gradients develop with depth, creating $O_2$-limited zones that facilitate nitritation.[114] Likewise, lower effective diffusivities of $NH_3$ and $O_2$ intensify NOB suppression.[111] Because DO penetration is gradient-limited, achieving high effluent $NO_2^-$ while maintaining satisfactory $NH_4^+$ conversion may require a higher bulk DO set-point.[115] The distributions of DO, substrates, and inhibitors (FA/FNA) are governed by biofilm thickness and the water–biofilm boundary layer. When the boundary layer exceeds ~50 μm, the NOB yield/AOB yield ratio falls below 0.33, indicating a substantial reduction of NOB biomass.[46] Consistent with these mechanisms, in continuous-flow PN granules, the AOB : NOB activity ratio increases with granule size under DO limitation alone, whereas in the presence of FA inhibition, the trend reverses and smaller granules (<150 μm) favor nitrite accumulation.[116] Carrier microstructure is equally consequential: conventional PVA/alginate beads with a dense outer skin restrict mass transfer and undermine PN/A stability, while enhanced DO diffusion within the matrix establishes micro-oxic gradients that selectively suppress NOB in pilot PN.[117]

Beyond operating conditions, community composition and relative abundances are also important for NOB suppression. A simple biokinetic assay on seed sludge (assessing AOB, NOB, and heterotrophs) was used to set a site-specific COD/N target for oxygen competition. In mainstream systems, a threshold of COD/N ≥3 repeatedly disadvantaged NOB, enriched heterotrophs, reduced *Nitrospira*, and stabilized PN, with findings confirmed in continuous reactors.[118] Consistent with this community preconditioning approach, another study demonstrated its operational translation in real-wastewater mixed consortia, showing that partial nitritation could be maintained with ~64–82% nitrite accumulation when aeration was controlled by an $NH_4^+$ set-point of 2–3 mg N $L^{-1}$, aerobic-phase DO was kept at 1.0–2.0 mg $L^{-1}$, and a post-anoxic step was implemented.[119]

*4.1.2.3 Precise control of R: $NO_2^-$-N : $NH_4^+$-N.* $O_2$ is the primary manipulated variable in PN. Aeration strategies—intermittent or continuous—are typically governed by DO.[120]

Open Access Article. Published on 05 ubat 2026. Downloaded on 12.05.2026 23:52:08.
This article is licensed under a Creative Commons Attribution-NonCommercial 3.0 Unported Licence.

An intelligent DO control scheme was used to realize SNAD. It combined a feed-forward module that computed and set the optimal DO set-point from multiple input variables with a feedback loop that kept DO within a prescribed range in real time.[121] Fine, flexible $O_2$ dosing can also be achieved by tuning water recirculation and water-spray at the gas–liquid interface to modulate oxygen transfer.[122] Besides direct DO/aeration control, pH and ORP were also used as a bend point.[123] During nitritation, proton release lowers pH while ORP rises. The bend point—where pH stops falling and begins to increase—signals the end of nitritation; ORP shows a corresponding inflection in the opposite direction. Detecting this point (*via* ΔpH, dpH/d*t*, or combined ORP, pH and DO signals) is key to stopping aeration in time and achieving the target R. However, bend-point behavior is sensitive to feed patterns, influent fluctuations, environmental changes, and sensor noise, so reliability is site-specific.[124]

Many plants instead use AVN control, tracking ammonia and nitrite to set aeration. This approach needs online *in situ* $NH_4^+$, $NO_2^-$, and $NO_3^-$ sensors and a dedicated controller.[125] In practice, high capital and maintenance costs, analyzer time delays, and poor discrimination between nitrate and nitrite have limited wider adoption.[125]

### 4.2 HAP-enhanced Anammox

**4.2.1 Low-temperature tolerance and adaptation of HAP–anammox granular systems.** A broad body of work on anammox indicates a clear temperature dependence of activity, with most studies reporting optimum temperatures in the warm-mesophilic range.[126,127] Reviews and experimental studies commonly report that the preferred operating temperature for unadapted anammox biomass is between 35 and 40 °C, with many systems operating stably in the range of 25 to 35 °C.[88,128,129]

Notably, lowering the temperature produces several well-documented negative effects on granular anammox systems. Short-term temperature drops reduce enzymatic rates and membrane-associated transport, causing sharp declines in anammox activity and nitrogen-removal rates,[10,130] and, depending on the history of the biomass, the decline may be reversible or may lead to slow recovery times. Furthermore, data from genome-centric metagenomics and metatranscriptomics reveal that low temperatures reprogram the transcriptional response of anammox consortia at the community level and select for cold-adapted strains, thereby altering their functional dynamics.[131] This leads to slower process kinetics and metabolic imbalances, potentiating the transient accumulation of intermediates such as $NO_2^-$ or NO under stress.

At low temperatures, HAP–anammox granular systems have demonstrated unexpectedly strong nitrogen-removal performance across multiple reactors and loading regimes. In an EGSB reactor seeded with HAP–anammox granules and operated at 7 °C for >200 days,[39] the NLR was ramped from 1.0 to 3.6 g N per L $d^{-1}$, achieving 84–92% nitrogen removal and yielding an apparent activation energy of 78.37 kJ $mol^{-1}$, which indicates preserved activity despite cold operation. Complementing this, a dedicated 7 °C study demonstrated that nitrogen-removal efficiency remained stable at ~82%, even as NLR reached 3.0 g N per L $d^{-1}$,[87] confirming that high-rate operation can be sustained at strictly low temperature. At 15 °C, a high-loading expanded-bed reactor achieved an NRR of 8.45 ± 0.49 g N per L $d^{-1}$ with >80% efficiency, while simultaneously recovering phosphorus as HAP,[88] further underscoring that HAP-mediated granulation supports both robust anammox performance and phosphorus capture under cold operation. The granule architecture of HAP–anammox supports a structure-ecology dual redundancy model in which the HAP core secures biomass retention and micro-environmental buffering, and the outer, AnAOB-rich layer preserves function, explaining the high NRR/NRE values observed at low temperatures.

**4.2.2 Stable performance of the HAP–anammox process under real wastewater conditions.** The HAP–anammox process has demonstrated remarkable robustness and

Table 3 The operational setup and performance of the HAP–anammox process

| Reactor type | Sludge type | Target wastewater | Temp. °C | Nitrogen Conc. mg N per L | NLR g N per L $d^{-1}$ | NRR g N per L $d^{-1}$ | HRT h | Nitrogen removal % | Ref. |
|---|---|---|---|---|---|---|---|---|---|
| EGSB | Hybrid | Synthetic wastewater | 35 | 800–1500 | 2.4–15.0 | 2.8–13.7 | 2–8 | 89–92 | 80 |
| UASB | Granule | Synthetic wastewater | 25 | 312–625 | 1.0–5.0 | 0.6–4.3 | 1–10 | 50–91 | 101 |
| EGSB | Granule | Synthetic wastewater | 15–35 | 625–1375 | 2.5–10.0 | 8.8 ± 0.1 | 1–6 | 80–90 | 88 |
| EGSB | Granule | Synthetic wastewater | 35 | 500–2000 | 3.0–20.0 | 2.7–13.4 | 2–5 | 88–91 | 92 |
| EGSB | Granule | Synthetic wastewater | 25 | 625–1500 | 5.0–11.0 | 16.7–17.1 | 12–3 | 84–90 | 84 |
| UAFB | Biofilm | Synthetic wastewater | 30 | 220–1000 | n.a. | n.a. | 6–13 | 76–84 | 136 |
| AAFEB | Granule | Synthetic wastewater | 35 | 200–500 | 0.8–10.0 | 8.4 ± 0.2 | 1–6 | 77 ± 4 | 59 |
| AAFEB | Biofilm | Synthetic wastewater | 35 | 313–1040 | 5.0–50.0 | 44.8 | 1–2 | 90 ± 1 | 58 |
| IC | Granule | Synthetic wastewater | 35 | 490–1490 | 1.4 | 1.34 | 8–24 | 66 ± 6 | 100 |
| EGSB | Granule | Synthetic wastewater | 7 | 251–513 | 1.0–3.6 | 0.9–3.1 | 2–6 | 73–92 | 39 |
| EGSB | Granule | Synthetic wastewater | 35 | 800 | 9.8 | 8.5 | 2 | 85–90 | 75 |
| UAHR | Hybrid | Synthetic wastewater | 25 | 241–720 | 0.7–3.0 | 0.39–1.85 | 8 | 71–90 | 35 |
| EGSB | Granule | Synthetic wastewater | 7 | 250–300 | 2.0–3.0 | 1.46–2.10 | 2–3 | 67–86 | 87 |
| AnMBR | Granule | Digestion wastewater | 25 | 1098–5219 | 1.2–15.4 | 0.80–14.9 | 6–12 | 89 ± 4 | 93 |
| EGSB | Granule | Fermentation wastewater | 25 | 236–1387 | 1.2–6.0 | 1.1–5.5 | 5 | 92 ± 1 | 40 |


This journal is © The Royal Society of Chemistry 2026

Open Access Article. Published on 05 ubat 2026. Downloaded on 12.05.2026 23:52:08.
This article is licensed under a Creative Commons Attribution-NonCommercial 3.0 Unported Licence.

efficiency when treating real wastewater, largely due to the hydroxyapatite-facilitated granulation that enhances settleability, biomass retention, and microbial resilience. The combination of mineral-driven granulation and a staged process architecture separates nitrification from the anammox stage, reducing inhibitory interactions and allowing the HAP–anammox stage to focus on efficient nitrite-driven $NH_4^+$ conversion with exceptional biomass retention and settleability.[11]

As shown in Table 3, compared with synthetic wastewater systems that are commonly used to demonstrate the feasibility and mechanisms of HAP–anammox processes, reactors operated with real wastewaters are typically subjected to higher nitrogen concentrations and more pronounced loading fluctuations. Synthetic wastewater systems generally operate with influent nitrogen levels ranging from 70 to 2000 mg $L^{-1}$ and achieve removal efficiencies between 70% and 95%. In comparison, HAP–anammox systems treating real wastewaters, such as anaerobic digestion liquor, fermentation effluent, or AnMBR permeate, often encounter much higher nitrogen concentrations (~200–5000 mg $L^{-1}$). Although these real-world systems do not reach the high NLRs achieved with synthetic wastewater (which can be as high as 50 g N per L $d^{-1}$), they still attain notable NLRs of up to 15.4 g N per L $d^{-1}$. More importantly, they achieve remarkable and stable nitrogen removal efficiencies of 89–92%. In addition, while synthetic systems are typically tested under mesophilic conditions (30–35 °C), which optimize anammox activity, systems treating real wastewater often operate at ambient or seasonally variable temperatures to better reflect practical implementation conditions.[93,132,133]

These results collectively highlight that, while synthetic wastewater studies provide mechanistic insight, the performance under real wastewater conditions demonstrates the robustness and engineering relevance of HAP–anammox granular systems, which can sustain high-strength nitrogen loads without sacrificing treatment efficiency.

## 5 Limitations and future works

For the PN step, at low temperature, nitrifier competition shifts and routine SRT/DO tactics often lose selectivity, making nitrite accumulation difficult to sustain. Seasonal swings further destabilize performance, and contributions from different nitrifier guilds (*e.g.*, AOB *vs.* AOA) can change with climate and operation. Future work should couple adaptive control with morphology management and strategies that enhance biomass retention. Mechanistic studies linking temperature, lineage traits, and mass transfer are needed to define reproducible low-temperature operating windows. Moreover, community composition strongly conditions NOB suppression, yet practical design rules remain site-specific. A promising direction is to pre-characterize seed sludge kinetics to set operations favoring the desired guilds. Research priorities include rational inoculation/bioaugmentation, quantifying lineage-specific sensitivities, and integrating multi-omics with biokinetic modeling to make community steering predictive and transferable.[134] For the HAP–A step, the feasibility of HAP recovery and reuse should be further explored. As HAP can act as a recyclable phosphorus resource, its regeneration and reintegration into the PN/HAP–anammox system may provide an additional pathway for circular nutrient management.[135,136] Economic factors, including the cost of HAP harvesting, separation, and reactivation, also warrant detailed evaluation. Moreover, the potential impacts of

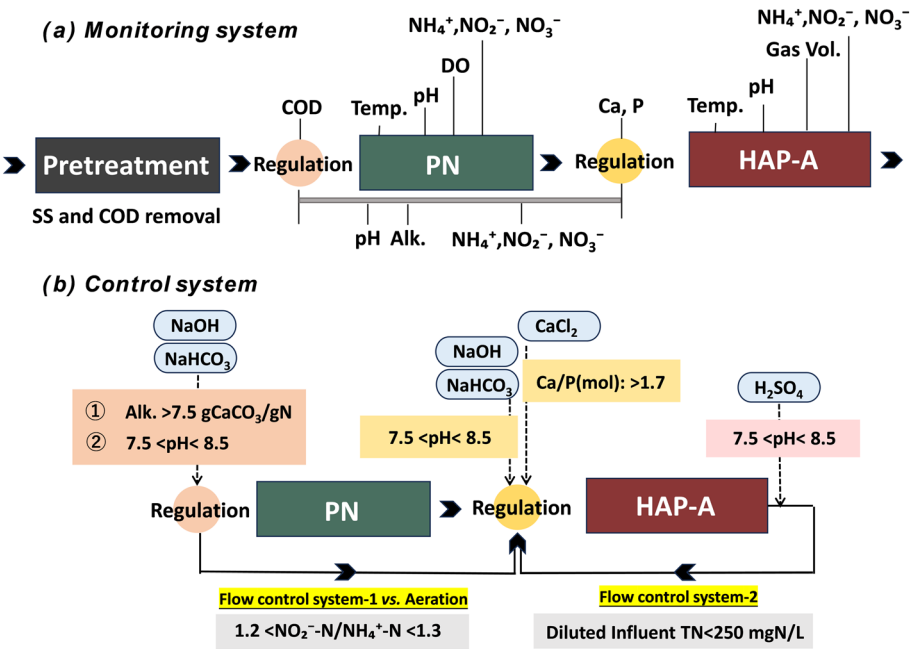


Fig. 3 Schematic of the monitoring system for two-stage PN/HAP–A (a) and the control system for two-stage PN/HAP–A (b).

Open Access Article. Published on 05 ubat 2026. Downloaded on 12.05.2026 23:52:08.
This article is licensed under a Creative Commons Attribution-NonCommercial 3.0 Unported Licence.

repeated HAP reuse on granule stability, microbial activity, and long-term process sustainability remain unclear and should be systematically investigated.

As an autotrophic train, the PN/HAP–A system is sensitive to organics, inhibitors, and solids, so many industrial matrices require pretreatment before reliable operation.[24,137] A modular toolbox that accounts for equalization, pH/alkalinity management, aerobic polishing, advanced oxidation, clarification, and membrane separation should be tailored to the wastewater and downstream constraints.[138,139] Notably, two-stage monitoring and control schemes are now relatively mature (Fig. 3). The next step is greater automation and sensitivity-self-calibrating analyzers, fault-tolerant data fusion, anomaly detection, and model-predictive or digital-twin-assisted control to handle dead time and drift.

## Conflicts of interest

There are no conflicts to declare.

## Abbreviations

| | |
|---|---|
| Anammox | Anaerobic ammonium oxidation |
| PN | Partial nitritation |
| PN/A | Partial nitritation–anammox |
| EBPR | Enhanced biological phosphorus removal |
| SNAD | Simultaneous partial nitrification, anammox, and denitrification |
| FA | Free ammonia |
| FNA | Free nitrous acid |
| AOA | Ammonia-oxidizing archaea |
| AOB | Ammonia-oxidizing bacteria |
| NOB | Nitrite-oxidizing bacteria |
| DO | Dissolved oxygen |
| MIM | Microbially induced mineralization |
| EPS | Extracellular polymeric substances |
| HAP | Hydroxyapatite |
| ACP | Amorphous calcium phosphate |
| DCPD | Dicalcium chosphate dihydrate (brushite) |
| OCP | Octacalcium phosphate |
| TCP | Tricalcium phosphate |
| SAA | Specific anammox activity |
| HRT | Hydraulic retention time |
| NLR | Nitrogen loading rate |
| NAR | Nitrite accumulative rate |
| NRR | Nitrogen removal rate |
| SRT | Solid retention time |
| R | The ratio of $NO_2^-$-N to $NH_4^+$-N |
| $\mu_{max}$ | The maximum specific growth rate |
| PN/PS | Protein-to-polysaccharide |
| $K_s$ | Half-saturation constant of substrate |
| $K_o$ | Half-saturation constant of $O_2$ |
| PSR | Pilot scale reactor |
| SBR | Sequencing batch reactor |
| CFB | Continuous flow bioreactor |
| MBSBBR | Moving bed sequencing batch biofilm reactor |
| ALR | Air-lift reactor |
| SBBR | Sequencing batch biofilm reactor |
| AGR | Air-lift granulation reactor |
| AnMBR | Anaerobic membrane bioreactors |
| cf-SBR | Continuous-fed sequencing batch reactor |
| UASB | Up-flow anaerobic sludge blanket |
| EGSB | Expanded granular sludge bed |
| CSTR | Continuous stirred tank reactors |
| EBR | Expanded bed reactor |
| UAFB | Up-flow anaerobic fixed-bed |
| AAFEB | Anammox attached film expanded bed |
| IC | Internal circulation |
| UAHR | Up-flow anammox hybrid reactor |

## Data availability

No new data were created or analyzed in this study. All statements are supported by previously published sources cited in the article. Any extraction sheets (*e.g.*, synthesized summary tables) generated during the review can be shared upon reasonable request.

## Acknowledgements

This study was supported by the Japan New Energy and Industrial Technology Development Organization (NEDO). This paper was supported by the open access promotion program of Tohoku University.

## References

1 L. Lu, J. S. Guest, C. A. Peters, X. Zhu, G. H. Rau and Z. J. Ren, *Nat. Sustain.*, 2018, **1**, 750–758.
2 Y. Zhang, D. Zhu, S. Zhou, H. Gong and X. Dai, *J. Hazard. Mater.*, 2025, **486**, 136967.
3 C. Rong, Y. Song, W. Yan, T. Zhang and Y. Y. Li, *Renewable Sustainable Energy Rev.*, 2025, **210**, 115154.
4 A. Joss, N. Derlon, C. Cyprien, S. Burger, I. Szivak, J. Traber, H. Siegrist and E. Morgenroth, *Environ. Sci. Technol.*, 2011, **45**, 9735–9742.
5 R. Du, S. Cao, H. Zhang, X. Li and Y. Peng, *Environ. Sci. Technol.*, 2020, **54**, 6353–6364.
6 B. Kartal, W. J. Maalcke, N. M. de Almeida, I. Cirpus, J. Gloerich, W. Geerts, H. J. M. Op den Camp, H. R. Harhangi, E. M. Janssen-Megens, K.-J. Francoijs, H. G. Stunnenberg, J. T. Keltjens, M. S. M. Jetten and M. Strous, *Nature*, 2011, **479**, 127–130.
7 S. Qiu, Z. Li, Y. Hu, L. Shi, R. Liu, L. Shi, L. Chen and X. Zhan, *Crit. Rev. Environ. Sci. Technol.*, 2021, **51**, 1045–1077.
8 S. K. Téllez-Pérez, S. Wyffels, H. KleinJan, C. Meunier and R. Gerards, *Chemosphere*, 2021, **280**, 130716.
9 Y. Liu, Y. Wu, Y. Zhao, J. Niu, Q. Wang, B. Bamanu, A. Hussain, Y. Liu, Y. Tong and Y. Y. Li, *Environ. Sci. Technol.*, 2024, **58**, 20768–20784.
10 C. Weralupitiya, R. Wanigatunge, S. Joseph, B. C. L. Athapattu, T. H. Lee, J. Kumar Biswas, M. P. Ginige, S.

 This journal is © The Royal Society of Chemistry 2026

Open Access Article. Published on 05 ubat 2026. Downloaded on 12.05.2026 23:52:08.
This article is licensed under a Creative Commons Attribution-NonCommercial 3.0 Unported Licence.

Shiung Lam, P. Senthil Kumar and M. Vithanage, *Bioresour. Technol.*, 2021, **334**, 125240.
11 Y. Song, Z. Ma, Y. Qin, W. Zhao, W.-K. Qi and Y.-Y. Li, *Resour., Conserv. Recycl.*, 2022, **184**, 106421.
12 H. Duan, L. Ye, Q. Wang, M. Zheng, X. Lu, Z. Wang and Z. Yuan, *Water Res.*, 2019, **162**, 331–338.
13 K. Fu, Y. Bian, F. Yang, J. Xu and F. Qiu, *J. Environ. Manage.*, 2023, **347**, 119186.
14 S. Cui, S. Ji, W. Zhao, L. Wan and Y. Y. Li, *Water Res.*, 2025, **276**, 123255.
15 R. Xiao, B. J. Ni, S. Liu and H. Lu, *Water Res.*, 2021, **191**, 116817.
16 Q. Zhang, S. E. Vlaeminck, C. DeBarbadillo, C. Su, A. Al-Omari, B. Wett, T. Pümpel, A. Shaw, K. Chandran, S. Murthy and H. De Clippeleir, *Water Res.*, 2018, **143**, 270–281.
17 K. Cho, S. Lee, J. Jung and D. Choi, *Environ. Res.*, 2023, **227**, 115748.
18 M. C. Li, Y. Song, W. Shen, C. Wang, W. K. Qi, Y. Peng and Y. Y. Li, *Bioresour. Technol.*, 2019, **293**, 122039.
19 T. Liu, Z. Khai Lim, H. Chen, S. Hu, Z. Yuan and J. Guo, *Environ. Sci. Technol.*, 2020, **54**, 3012–3021.
20 W. J. Ma, Z. Q. Ren, L. Q. Yu, X. X. Wu, Y. X. Yao, J. T. Zhang, J. Y. Guo, N. S. Fan and R. C. Jin, *Chem. Eng. J.*, 2021, **426**, 130815.
21 G. F. Li, W. J. Ma, Z. Q. Ren, Y. Wang, J. P. Li, J. W. Zhao, S. T. Li, Q. Liu, Y. N. Gu, Y. F. Cheng, B. C. Huang and R. C. Jin, *Environ. Sci. Technol.*, 2021, **55**, 16627–16635.
22 D. Xu, C. Pan, W. Chen, P. Zheng, M. Zhang and Z. Wang, *Environ. Sci. Technol.*, 2024, **58**, 19353–19361.
23 T. Oh, Y. Choi, J. Kim, Y. Lim, M. Jung and Y. Choi, *J. Water Process Eng.*, 2025, **75**, 107985.
24 D. Valenzuela-Heredia, C. Panatt, M. Belmonte, O. Franchi, D. Crutchik, J. Dumais, J. R. Vázquez-Padín, Y. Lesty, A. Pedrouso, Á. Val del Río, A. Mosquera-Corral and J. L. Campos, *Chem. Eng. J.*, 2022, **429**, 131301.
25 Y. Xue, H. Ma, Y. Hu, Z. Kong and Y. Y. Li, *Water Res.*, 2022, **210**, 117968.
26 Y. Song, Y. Huang, Z. Ma, J. Ni, T. Zhang and Y. Y. Li, *Chem. Eng. J.*, 2024, **502**, 157765.
27 H. Shi, X. Ren, R. Yang, J. Wang, H. Xu, X. Liao, Y. Lou, S. Chen, X. Ye and X. Wang, *Water Res.*, 2025, **272**, 122954.
28 Y. Chen, G. Feng, G. Guo, K. Urasaki, K. Kubota and Y. Y. Li, *Environ. Sci. Technol.*, 2023, **57**, 7624–7633.
29 Y. M. Lin, T. Lotti, P. K. Sharma and M. C. M. van Loosdrecht, *Water Res.*, 2013, **47**, 4556–4566.
30 Y. Qian, Y. Guo, J. Shen, Y. Qin and Y. Y. Li, *Water Res.*, 2022, **217**, 118437.
31 Y. Song, L. Lin, W. K. Qi, O. Sasaki and Y. Y. Li, *Environ. Sci. Technol.*, 2023, **57**, 10242–10251.
32 Y. Guo, T. Sugano, Y. Song, C. Xie, Y. Chen, Y. Xue and Y. Y. Li, *Bioresour. Technol.*, 2020, **311**, 123489.
33 Y. Guo and Y. Y. Li, *Water Res.*, 2020, **187**, 116444.
34 Y. Xue, H. Ma, Z. Kong and Y. Y. Li, *Water Res.*, 2021, **193**, 116861.
35 Y. Song, J. Ni, Y. Guo, K. Kubota, W. K. Qi and Y. Y. Li, *Chemosphere*, 2023, **313**, 137580.
36 J. Liu, M. Zheng, C. Wang, C. Liang, Z. Shen and K. Xu, *Resour., Conserv. Recycl.*, 2020, **157**, 104793.
37 Z. Z. Zhang, J. J. Xu, H. Y. Hu, Z. J. Shi, Z. Q. Ji, R. Deng, M. L. Shi and R. C. Jin, *Bioresour. Technol.*, 2016, **208**, 161–169.
38 Y. Song, Z. Ma, Y. Qin, W. Zhao, W.-K. Qi and Y.-Y. Li, *Resour., Conserv. Recycl.*, 2022, **184**, 106421.
39 Y. Song, L. Lin, J. Ni, H. Ma, W. K. Qi and Y. Y. Li, *Water Res.*, 2021, **206**, 117764.
40 Y. Song, Z. Ma, R. Du, Y. Guo, Y. Qin, J. Tanno, W.-K. Qi and Y.-Y. Li, *Bioresour. Technol.*, 2022, **344**, 126238.
41 J. Hou, Y. Zhu, Y. Shi, L. Lin, F. Meng, M. Xu, L. Yang, B.-J. Ni and X. Chen, *Environ. Sci. Technol.*, 2025, **59**, 15272–15281.
42 X. Ran, T. Wang, M. Zhou, Z. Li, H. Wang, G. T. Tsybekmitova, J. Guo and Y. Wang, *Environ. Sci. Technol.*, 2025, **59**, 8922–8938.
43 Y. Ye, W. Xiong, S. He, Y. Xiang, J. Xiao, W. Feng, Z. Yang, D. He and D. Wang, *Environ. Sci. Technol.*, 2025, **59**, 16753–16763.
44 J. Dosta, I. Fernández, J. R. Vázquez-Padín, A. Mosquera-Corral, J. L. Campos, J. Mata-Álvarez and R. Méndez, *J. Hazard. Mater.*, 2008, **154**, 688–693.
45 R. Salvetti, A. Azzellino, R. Canziani and L. Bonomo, *Water Res.*, 2006, **40**, 2981–2993.
46 X. Liu, M. Kim, G. Nakhla, M. Andalib and Y. Fang, *J. Environ. Chem. Eng.*, 2020, **8**, 103984.
47 K. Dimitri Kits, C. J. Sedlacek, E. V. Lebedeva, P. Han, A. Bulaev, P. Pjevac, A. Daebeler, S. Romano, M. Albertsen, L. Y. Stein, H. Daims and M. Wagner, *Nature*, 2017, **549**, 269–272.
48 H. D. Park and D. R. Noguera, *J. Appl. Microbiol.*, 2007, **102**, 1401–1417.
49 S. G. Kantartzi, E. Vaiopoulou, A. Kapagiannidis and A. Aivasidis, *Global NEST J.*, 2006, **8**, 43–51.
50 A. Terada, S. Sugawara, T. Yamamoto, S. Zhou, K. Koba and M. Hosomi, *Biochem. Eng. J.*, 2013, **79**, 153–161.
51 T. G. L. Vandekerckhove, F. M. Kerckhof, C. De Mulder, S. E. Vlaeminck and N. Boon, *Water Res.*, 2019, **156**, 34–45.
52 S. E. Vlaeminck, A. Terada, B. F. Smets, H. De Clippeleir, T. Schaubroeck, S. Bolea, L. Demeestere, J. Mast, N. Boon, M. Carballa and W. Verstraete, *Appl. Environ. Microbiol.*, 2010, **76**, 900–909.
53 C. Combes and C. Rey, *Acta Biomater.*, 2010, **6**, 3362–3378.
54 H. Dai, X. Lu, Y. Peng, Z. Yang and H. Zhsssu, *Environ. Sci. Pollut. Res.*, 2017, **24**, 5791–5799.
55 S. V. Dorozhkin, *Biomaterials*, 2010, **31**, 1465–1485.
56 F. Wu, D. D. W. Lin, J. H. Chang, C. Fischbach, L. A. Estroff and D. Gourdon, *Cryst. Growth Des.*, 2015, **15**, 2452–2460.
57 S. G. Da Cruz, M. B. D. M. Monte and A. J. B. Dutra, *Braz. J. Chem. Eng.*, 2017, **34**, 821–830.
58 Y. Zhang, H. Ma, L. Lin, W. Cao, T. Ouyang and Y.-Y. Li, *ACS Sustainable Chem. Eng.*, 2018, **6**, 10989–10998.
59 L. Lin, Y. Zhang, M. Beckman, W. Cao, T. Ouyang, S. Wang and Y.-Y. Li, *Bioresour. Technol.*, 2019, **290**, 121779.
60 M. H. Santos, M. De Oliveira, L. Palhares, F. Souza, H. S. Mansur and L. Vasconcelos, *Mater. Res.*, 2004, **7**, 625–630.

Open Access Article. Published on 05 ubat 2026. Downloaded on 12.05.2026 23:52:08.
This article is licensed under a Creative Commons Attribution-NonCommercial 3.0 Unported Licence.

61 S. Hajimirzaee, S. Chansai, C. Hardacre, C. E. Banks and A. M. Doyle, *J. Solid State Chem.*, 2019, **276**, 345–351.
62 L. Cao, Y. He, Y. Y. Li, Z. Kong, H. Jiang, Y. Hu and X. Zhang, *Environ. Res.*, 2025, **266**, 120605.
63 H. Ma, Y. Zhang, Y. Xue and Y. Y. Li, *Bioresour. Technol.*, 2018, **267**, 201–208.
64 A. Lotsari, A. K. Rajasekharan, M. Halvarsson and M. Andersson, *Nat. Commun.*, 2018, **9**, 4170.
65 J. A. Stammeier, B. Purgstaller, D. Hippler, V. Mavromatis and M. Dietzel, *MethodsX*, 2018, **5**, 1241–1250.
66 S. Tang, Z. Dong, X. Ke, J. Luo and J. Li, *Int. J. Oral Sci.*, 2021, **13**, 42.
67 J. R. Cunha, C. Schott, R. D. van der Weijden, L. H. Leal, G. Zeeman and C. Buisman, *Environ. Res.*, 2019, **178**, 108671.
68 J. R. Cunha, S. Morais, J. C. Silva, R. D. Van Der Weijden, L. Hernández Leal, G. Zeeman and C. J. N. Buisman, *Environ. Sci. Technol.*, 2019, **53**, 1334–1343.
69 J. R. Cunha, T. Tervahauta, R. D. Van Der Weijden, H. Temmink, L. Hernández Leal, G. Zeeman and C. J. N. Buisman, *Environ. Sci. Technol.*, 2018, **52**, 13144–13154.
70 F. Xiong, D. Wen and Q. Li, *Front. Environ. Sci.*, 2022, **10**, 815528.
71 J. Zhen, Q. Cui, X. Liu, Z. Yu, C. Wang and S. Q. Ni, *Bioresour. Technol.*, 2021, **340**, 125729.
72 Y. Kim, J. Yu, S. Jeong, J. Kim, S. Park, H. Bae, S.-K. Rhee, T. Unno, S.-Q. Ni and T. Lee, *Appl. Sci.*, 2021, **12**, 19.
73 Z. Li, D. Li, H. Guo, J. Zhang, W. Wang, H. Zeng and J. Zhang, *Chem. Eng. J.*, 2023, **474**, 146020.
74 Y. Xue, H. Ma and Y. Y. Li, *Water Res.*, 2023, **228**, 119353.
75 L. Liang, J. Luo, X. Xiao, J. Wang, M. Hong, C. Deng, Y. Y. Li and J. Liu, *Sci. Total Environ.*, 2022, **805**, 150359.
76 W. Wang, J. Wang, H. Wang, J. Ma, M. Wu and Y. Wang, *Water Res.*, 2020, **187**, 116454.
77 A. Magrí, E. Company, F. Gich and J. Colprim, *ACS Sustainable Chem. Eng.*, 2021, **9**, 2745–2761.
78 W. Xu, T. Zhang, J. Wan, H. Li, Y. Chen and Y. Wang, *Bioresour. Technol.*, 2021, **326**, 124628.
79 S. Ji, S. Cui, H. Zhao, H. Qin, Y. Qin, Y. Chen and Y. Y. Li, *Chem. Eng. J.*, 2025, **522**, 166927.
80 L. Lin, Y. Song, Y. Zhang, Z. Luo, Q. Li, W. Cao and Y. Y. Li, *Bioresour. Technol.*, 2024, **406**, 131091.
81 Y. Xue, H. Ma, Z. Kong, Y. Guo and Y. Y. Li, *Bioresour. Technol.*, 2020, **310**, 123421.
82 H. Chen, H. Y. Hu, Q. Q. Chen, M. L. Shi and R. C. Jin, *Bioresour. Technol.*, 2016, **211**, 594–602.
83 Y. F. Cheng, Z. Z. Zhang, G. F. Li, Q. Zhang, X. P. Zheng, S. Cai, Y. Xue, B. C. Huang and R. C. Jin, *Environ. Sci. Technol.*, 2020, **54**, 12959–12966.
84 H. Ma, Y. Xue, Y. Zhang, T. Kobayashi, K. Kubota and Y. Y. Li, *Water Res.*, 2020, **172**, 115510.
85 C. Polizzi, T. Lotti, A. Ricoveri, R. Campo, C. Vannini, M. Ramazzotti, D. Gabriel and G. Munz, *J. Environ. Chem. Eng.*, 2022, **10**, 107002.
86 M. Yuan, Q. Shan, M. Fu, M. Deng, J. Wang and F. Deng, *Chemosphere*, 2024, **350**, 141158.
87 L. Lin, Y. Song and Y. Y. Li, *Chem. Eng. J.*, 2022, **433**, 133644.
88 H. Ma, Y. Zhang, Y. Xue, K. Kubota and Y. Y. Li, *Chem. Eng. J.*, 2021, **425**, 130636.
89 J. Luo, H. Chen, X. Han, Y. Sun, Z. Yuan and J. Guo, *FEMS Microbiol. Ecol.*, 2017, **93**, 21.
90 V. Kouba, K. Hůrková, K. Navrátilová, D. Kok, A. Benáková, M. Laureni, P. Vodičková, T. Podzimek, P. Lipovová, L. van Niftrik, J. Hajšlová, M. C. M. van Loosdrecht, D. G. Weissbrodt and J. Bartáček, *Chem. Eng. J.*, 2022, **445**, 136712.
91 J. Xie, T. An, A. Mabruk, Y. Wang, T. C. Zhang, J. Wang and C. Chen, *J. Cleaner Prod.*, 2023, **385**, 135757.
92 L. Lin, K. Ishida, Y. Zhang, N. Usui, A. Miyake, N. Abe and Y.-Y. Li, *Sci. Total Environ.*, 2023, **857**, 159719.
93 L. Lin, W. Zhao, S. Cui, Y. Song, Y. Zhang and Y. Y. Li, *J. Water Process Eng.*, 2025, **72**, 107642.
94 L. Lin, Z. Luo, K. Ishida, K. Urasaki, K. Kubota and Y. Y. Li, *Water Res.*, 2022, **221**, 118751.
95 Z. Li, D. Li, J. Zhang, W. Wang, M. Li, S. Wang, H. Zeng and J. Zhang, *J. Water Process Eng.*, 2024, **59**, 105083.
96 P. Bovio-Winkler, L. D. Guerrero, L. Erijman, P. Oyarzúa, M. E. Suárez-Ojeda, A. Cabezas and C. Etchebehere, *BMC Microbiol.*, 2023, **23**, 1–19.
97 C. E. Lawson, S. Wu, A. S. Bhattacharjee, J. J. Hamilton, K. D. McMahon, R. Goel and D. R. Noguera, *Nat. Commun.*, 2017, **8**, 1–12.
98 N. S. Fan, Y. H. Bai, J. Wu, Q. Zhang, J. J. Fu, W. L. Zhou, B. C. Huang and R. C. Jin, *J. Cleaner Prod.*, 2020, **261**, 121148.
99 T. Okubo and H. Takami, *Microbiology*, 2021, **10**, e1227.
100 L. Chen, Z. Wu, J. Niu, Y. Wang, M. Cai, J. Xi, Y. Cui, L. Cheng and X. Fan, *Bioresour. Technol.*, 2025, **419**, 132045.
101 L. Wei, Y. Hu, Y. Xue, W. Tian, Y. Xue and R. Chen, *J. Water Process Eng.*, 2024, **64**, 105582.
102 H. Ma, Q. Niu, Y. Zhang, S. He and Y. Y. Li, *Bioresour. Technol.*, 2017, **238**, 263–272.
103 Y. Xue, M. Zheng, Z. Cheng, S. Li, S. Yang, Y. Liu, Y. Qian and X. Huang, *Environ. Sci. Technol.*, 2023, **57**, 17542–17552.
104 S. Li, X. Kang, Z. Zuo, M. S. Islam, S. Yang, Y. Liu and X. Huang, *Water Res.*, 2024, **262**, 122078.
105 M. Muszyński-Huhajło, K. Ratkiewicz, K. Janiak, S. Miodoński, A. Jurga and R. Szetela, *J. Environ. Chem. Eng.*, 2022, **10**, 106995.
106 T. L. G. Hendrickx, Y. Wang, C. Kampman, G. Zeeman, H. Temmink and C. J. N. Buisman, *Water Res.*, 2012, **46**, 2187–2193.
107 E. M. Gilbert, S. Agrawal, F. Brunner, T. Schwartz, H. Horn and S. Lackner, *Environ. Sci. Technol.*, 2014, **48**, 2934–2941.
108 G. K. Hassan and F. A. El-Gohary, *Water, Air, Soil Pollut.*, 2021, **232**, 1–12.
109 V. M. Vadivelu, J. Keller and Z. Yuan, *Biotechnol. Bioeng.*, 2006, **95**, 830–839.
110 W. Qian, Y. Peng, X. Li, Q. Zhang and B. Ma, *Bioresour. Technol.*, 2017, **243**, 1247–1250.

 This journal is © The Royal Society of Chemistry 2026

Open Access Article. Published on 05 ubat 2026. Downloaded on 12.05.2026 23:52:08.
This article is licensed under a Creative Commons Attribution-NonCommercial 3.0 Unported Licence.

111 S. Li, H. Duan, Y. Zhang, X. Huang, Z. Yuan, Y. Liu and M. Zheng, *Sci. Total Environ.*, 2020, **728**, 138713.
112 H. Duan, L. Ye, X. Lu and Z. Yuan, *Environ. Sci. Technol.*, 2019, **53**, 1937–1946.
113 X. Hu, J. Song, Y. Ji, C. Li, J. Wei, W. Lyu, B. Wang, W. Guo, R. Chen, H. Wang, D. Zhou and Q. Zhang, *Chin. Chem. Lett.*, 2023, **34**, 108284.
114 P. Kunapongkiti, C. Rongsayamanont, P. Nayramitsattha and T. Limpiyakorn, *Environ. Eng. Res.*, 2020, **25**, 807–818.
115 M. Soliman and A. Eldyasti, *Rev. Environ. Sci. Bio/Technol.*, 2018, **17**, 285–321.
116 T. R. Kent, Y. Sun, Z. An, C. B. Bott and Z. W. Wang, *Environ. Int.*, 2019, **131**, 105005.
117 D. Choi and J. Jung, *J. Water Process Eng.*, 2022, **48**, 102921.
118 W. Yun, K. Cho, J. Jung and D. Choi, *J. Water Process Eng.*, 2023, **53**, 103650.
119 L. Smoot, J. Mellin, C. K. Brinkman, I. Popova and E. R. Coats, *Water Res.*, 2022, **224**, 119074.
120 W. Zhou, Q. Zhang, B. Wang, Y. Peng, F. Hou, H. Pang and Y. Peng, *Water Res.*, 2025, **268**, 122615.
121 X. Wen, B. Gong, J. Zhou, Q. He and X. Qing, *Water Res.*, 2017, **119**, 201–211.
122 S. Qiu, Z. Li, X. Sheng, S. Wang, Y. Hu, A. B. de Menezes, L. Chen, R. Liu and X. Zhan, *Water Res.*, 2020, **185**, 116213.
123 S. Ji, R. Wu, Y. Zhang, H. Zhao, H. Qin, J. Liu and Y. Y. Li, *Bioresour. Technol.*, 2025, **432**, 132676.
124 F. Jaramillo, M. Orchard, C. Muñoz, M. Zamorano and C. Antileo, *J. Environ. Manage.*, 2018, **218**, 154–164.
125 P. Regmi, M. W. Miller, B. Holgate, R. Bunce, H. Park, K. Chandran, B. Wett, S. Murthy and C. B. Bott, *Water Res.*, 2014, **57**, 162–171.
126 P. Wu, J. Chen, V. K. Garlapati, X. Zhang, F. W. V. Jenario, X. Li, W. Liu, C. Chen, T. M. Aminabhavi and X. Zhang, *Chem. Eng. J.*, 2022, **444**, 136534.
127 M. Adams, J. Xie, A. W. J. Kabore, Y. Chang, J. Xie, M. Guo and C. Chen, *Crit. Rev. Environ. Sci. Technol.*, 2022, **52**, 631–674.
128 D. Sobotka, J. Zhai and J. Makinia, *Sci. Total Environ.*, 2021, **775**, 145760.
129 A. D. Pereira, A. Cabezas, C. Etchebehere, C. A. de L. Chernicharo and J. C. de Araújo, *Environ. Technol. Rev.*, 2017, **6**, 74–93.
130 X. Chen, L. Liu, Y. Bi, F. Meng, D. Wang, C. Qiu, J. Yu and S. Wang, *Environ. Res.*, 2023, **223**, 115464.
131 R. Niederdorfer, D. Hausherr, A. Palomo, J. Wei, P. Magyar, B. F. Smets, A. Joss and H. Bürgmann, *Commun. Biol.*, 2021, **4**, 23.
132 Y. Guo, Z. Luo, C. Rong, T. Wang, Y. Qin, T. Hanaoka, S. Sakemi, M. Ito, S. Kobayashi, M. Kobayashi and Y. Y. Li, *Sci. Total Environ.*, 2022, **807**, 151063.
133 J. Wu, Z. Kong, Z. Luo, Y. Qin, C. Rong, T. Wang, T. Hanaoka, S. Sakemi, M. Ito, S. Kobayashi, M. Kobayashi, K. Q. Xu, T. Kobayashi, K. Kubota and Y. Y. Li, *Water Res.*, 2021, **207**, 117783.
134 L. Yang, H. Yao, F. Jia, B. Han, Y. Chen, J. Jiang, T. Liu and J. Guo, *Water Res.*, 2023, **244**, 120524.
135 W. Xiao, Y. Hu, S. Li, J. Shi, W. Tian, Y. Xue and R. Chen, *J. Environ. Chem. Eng.*, 2025, **13**, 115759.
136 J. Wan, Z. Zhang, P. Li, Y. Ma, H. Li, Q. Guo, Y. Wang and C. Dagot, *Chemosphere*, 2024, **350**, 141040.
137 Y. Chen, H. Chen, Z. Chen, H. Hu, C. Deng and X. Wang, *J. Environ. Manage.*, 2021, **292**, 112762.
138 Z. Yan, A. Li, H. Shim, D. Wang, S. Cheng, Y. Wang and M. Li, *J. Environ. Manage.*, 2022, **317**, 115470.
139 S. Cao, R. Du and Y. Zhou, *Bioresour. Technol.*, 2022, **356**, 127310.